

Chemical disorder as engineering tool for spin-polarization in Mn_3Ga -based Heusler systems

S. Chadov,¹ S. W. D'Souza,¹ L. Wollmann,¹ J. Kiss,¹ G. H. Fecher,¹ and C. Felser¹

¹*Max-Planck-Institut für Chemische Physik fester Stoffe, 01187 Dresden, Germany*

Our study highlights spin-polarization mechanisms in metals, by focusing on the mobilities of conducting electrons with different spins instead of their quantities. Here, we engineer electron mobility by applying chemical disorder induced by non-stoichiometric variations. As a practical example, we discuss the scheme that establishes such variations in tetragonal Mn_3Ga Heusler material. We justify this approach using first-principles calculations of the spin-projected conductivity components based on the Kubo-Greenwood formalism. It follows that, in majority of the cases, even a small substitution of some other transition element instead of Mn may lead to a substantial increase in spin-polarization along the tetragonal axis.

PACS numbers: 72.15.Eb, 72.15.Gd, 72.25.Ba, 73.20.Fz

Keywords: electron localization, conductivity, spin-polarization, constructive disorder

I. INTRODUCTION

Improved understanding of the influence of disorder in solids yields potential new approaches to the state-of-the-art design of multicomponent materials. Despite the popular view that disorder should be avoided by any means, one can find its constructive influence on physical properties in various applied fields. Examples include the disorder-induced mechanical work hardening of materials [1], “softer” examples such as the efficient blocking of sound waves in liquid foams [2], and the Anderson localization of light in disordered photonic crystals [3]. By carefully reviewing the literature, one finds many more constructive examples. Constructive disorder simply prevents the propagation of certain quasiparticles. Indeed, in the first example, mechanical dislocations are blocked by other type of random defects; in the second, ultrasonic phonons are blocked by random foam bubbles; and in the third, electromagnetic waves are blocked by the breaking of the translational symmetry in the photonic crystal. Of course, similar phenomena also accompany electronic propagation in metals, where the breaking of translational symmetry (static or dynamic) leads to a nonzero resistivity. Here, one of the most dramatic examples is the Anderson localization [4, 5], which completely blocks the propagation of an electron despite the absence of a semiconducting gap in the density of states. This can have constructive implications, for example, it has recently been proposed that Anderson localization induced in topologically non-trivial systems, such as HgTe-type semimetals, should result in a new class of topological insulator [6–8]. On the other hand, in “typical” metals (i.e., systems with a conducting electron density of $n_F \gtrsim 5 \times 10^{22} \text{ cm}^{-3}$), the Anderson-Mott criterion [9] ($a_B n_F^{1/3} < 0.25$, where a_B is the Bohr radius) cannot be fulfilled, so an unlimited increase in disorder leads to a saturation of metallic resistivity which, in practice, is restricted by the empirical Mooij limit, $\rho_{\text{max}} \lesssim 300 \mu\Omega\text{cm}$ [10].

Here, we would like to demonstrate another interesting

effect that can be induced by disorder in metallic systems, the so-called *spin-selective* electron localization. Specifically, we will justify the possibility of creating such a type of disorder, which noticeably localizes the conducting electrons of one spin but almost negligibly affects the conduction of the other spin. It is rather clear that, since the spin subbands in a magnetic metal are different, their conductivities also differ (i.e. $\sigma^\uparrow \neq \sigma^\downarrow$). The extreme case, which is especially interesting in terms of spintronics, is the half-metallicity (i.e. $\sigma^\uparrow > 0$, $\sigma^\downarrow = 0$ or vice versa) characterized by the highest possible amplitude of the spin-polarization, $P = \frac{\sigma^\uparrow - \sigma^\downarrow}{\sigma^\uparrow + \sigma^\downarrow} = \pm 1$. It can be realized in the special class of materials known as half-metals [11, 12], which possess a semiconducting band gap in one spin channel only (i.e. $n_F^\uparrow = 0$, $n_F^\downarrow > 0$ or vice versa). However, as one can see in the simple Drude picture, $\sigma \sim n_F l$. Thus, the conductivity also scales with an electronic mean free path l , providing the potential for $P = \frac{n_F^\uparrow l^\uparrow - n_F^\downarrow l^\downarrow}{n_F^\uparrow l^\uparrow + n_F^\downarrow l^\downarrow}$, to be adjusted by manipulation of the electron mobilities, $l^{\uparrow(\downarrow)}$, in different spin channels, rather than adjusting the $n_F^{\uparrow(\downarrow)}$ only.

A large number of mechanisms exist that favor the disorder in solids provided by a diverse manifold of the degrees of freedom, whether thermal (such as phonons, magnons, polarons) or fully intrinsic (such as through geometrical frustration, stoichiometric variations and electron interaction). In order to engineer such mechanisms efficiently, one must understand their impact on the electronic structure. At present, certain connections can be established using special mean-field theories (e.g. coherent potential approximation (CPA) [13, 14] or dynamical mean-field theory (DMFT) [15, 16]), statistical methods (e.g. Monte-Carlo-based simulations) or combined approaches.

Here, we will restrict our engineering to a very fundamental level by improving the ground-state electronic transport characteristics through a particular type of chemical disorder, as it is one of the most common phenomena in polyatomic solid compositions. The simplest

way to introduce chemical disorder is through variation of the stoichiometry. Here, a convenient test environment is provided by the Heusler family of materials, which typically have a ternary composition: two different transition metals (TM) and one main-group element (MG). The majority of these substances crystallize in the fcc-based cubic structure (centrosymmetric $Fm-3m$ or noncentrosymmetric $F-43m$) and obey the same chemical ordering rules [17]. By substituting one TM for another TM or one MG by another MG, the properties of Heusler materials can be varied widely without affecting their structure, from nonmagnetic/semiconducting to magnetic/metallic. In particular, the latter class includes the majority of the known half-metals as given in Refs. [11, 12]. A nonstoichiometric substitution will lead to a random occupation of the corresponding Wyckoff sites, by automatically breaking the translational invariance. This random site occupation by two or more elements with localized electronic subbands (e.g. $3d$ states) centered at different energies will disturb the coherent scattering of the delocalized (mobile) electrons at corresponding energies and result in their partial localization. Thus, if the nonstoichiometric substitution induces these random fluctuations within the energy window containing the Fermi level (E_F), the resistivity will increase. The concept is therefore clear; we must create such an energy window at E_F in one spin channel, and simultaneously shift it away from E_F in the other channel. Such a situation can be maintained, obviously, only in magnetic systems.

II. RANDOM FLUCTUATION DESIGN: Mn_3Ga AND ITS DERIVATIVES

We select Mn_3Ga Heusler as a suitable object, since it possesses strong local moments and is not a half-metal. This is because of its tetragonal distortion which reduces its point symmetry to $I4/mmm$. Chemically speaking it is a binary, however, it contains two types of Mn in the $2a$ and $4c$ Wyckoff positions (marked red and blue, respectively, in Fig. 1 a) which differ by their nearest neighbor environment. $Mn(2a)$ has the largest local moment (according to different measurements and first-principles estimations $\approx 3-4 \mu_B$) coupled antiparallel to $Mn(4c)$, which has a smaller moment of $\approx 2-3 \mu_B$. Since the $4c$ class contains two Mn atoms (in $2c$ and $2d$, which are equivalent), the total magnetization, M , is oriented along the $4c$ local moments. $M \approx 1.7 \mu_B/\text{f.u.}$ (f.u.=formula unit) according to the first-principles calculation (see, e.g., [18]), and $M \approx 1.1 \mu_B/\text{f.u.}$ according to experiment [19–21] (note that the saturation was not achieved).

Let us examine the energetic structures of our future scattering centers (localized $3d$ states of Mn). They are shown schematically in Fig. 1 a. $Mn(2a)$, which exhibits the strongest magnetic moment, is close to the half-filled state. Its $3d$ shell contains five spin-down electrons, whereas the spin-up states are empty (ideally this

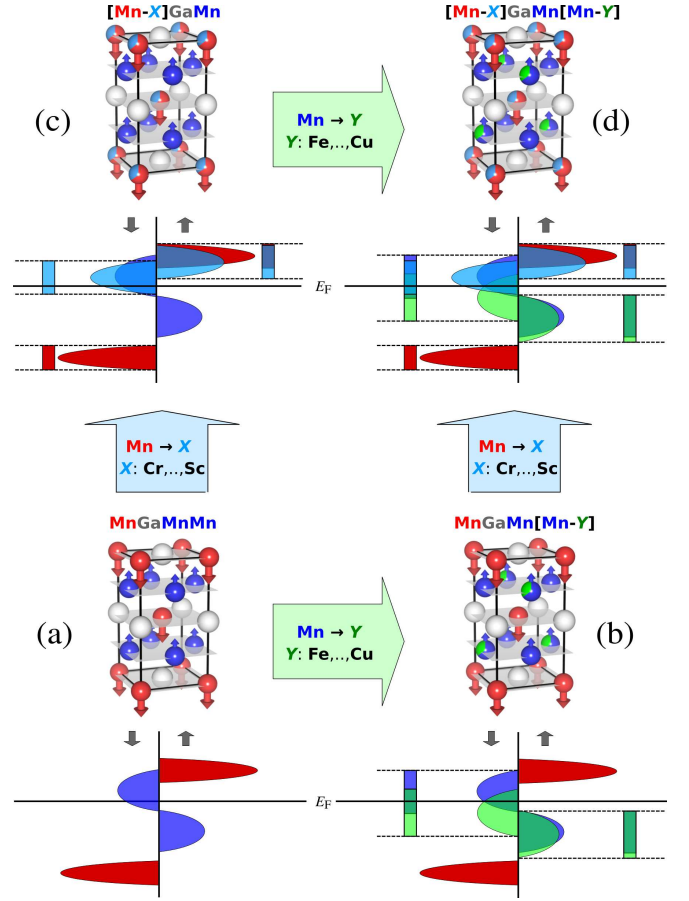


FIG. 1: (a) Mn_3Ga unit cell: Mn atoms in the $2a$ (red) and $2c/2d = 4c$ (blue) Wyckoff sites; Ga atoms are in $2b$ (gray); arrows indicate atomic magnetic moments. According to the sequence of Wyckoff positions, $2a\ 2b\ 2c\ 2d$, we label this compound as $MnGaMnMn$. (b) Substituting a late TM in place of Mn (Y, light-green) results in a $MnGaMn[Mn-Y]$ alloy with Mn-Y disorder on $2d$ sites. (c) Replacing Mn with an early TM (X, light-blue) results in a $[Mn-X]GaMnMn$ alloy with Mn-X disorder on $2a$. (d) Simultaneous combination of (b) and (c): $[Mn-X]GaMn[Mn-Y]$. The corresponding spin-projected and atomic-resolved $3d$ -DOS scheme for each prototype system (left-oriented peaks are spin-down, right-oriented are spin-up, as indicated by gray arrows). The atom-projected DOS contributions obey the same color code as that used for the atoms; vertical colored bars indicate the energy windows in which the electronic levels randomly fluctuate.

should result in $5 \mu_B$, however, this can differ in calculations, since the amplitude of the local moment depends on the position at which the “border” between the atoms is set). On the other hand, $Mn(4c)$ exhibits a smaller moment and weaker exchange split; this simply means that, whereas the spin-up band is fully filled, the spin-down band is not fully empty, i.e., it contains E_F . Such a “half-metallic” structure of the localized electronic subsystem (the delocalized s and p conducting electrons, which are not shown in the scheme, do not have a band gap in any of the spin channels) fits well into the framework of the

Anderson impurity model [22], which explains the spin dependence of the conducting electron scattering on a given magnetic impurity. In the second-order perturbation theory, the scattering process involves an intermediate state in which a conducting electron occupies an impurity level. At E_F , this is a partially filled spin-down $3d$ subband of $\text{Mn}(4c)$. According to the Pauli exclusion principle, intermediate states in which the impurity level is occupied by two electrons with the same spin orientation are forbidden. Thus, the spin-down conducting electrons will be repelled from the $\text{Mn}(4c)$ spin-down subband more strongly, which results in a relative increase in the spin-down resistivity component, ρ^\downarrow . The only ingredient which is still missing is the chemical disorder on the $4c$ sites, which leads to a random fluctuation of the spin-down localized d -electron subband by causing it to become an efficient scattering center.

This type of disorder can be introduced by substituting some other TM in place of Mn. One of the general rules, that holds quite unambiguously for Heusler alloys concerns their chemical ordering (see e.g. [17]). Specifically, the *earliest* TM (which is located closer to the left side of the periodic table, i.e., which belongs to the earliest group) shares the same atomic layer as the MG element (e.g., if Ga occupies $2b$, the earliest TM occupies the $2a$ Wyckoff site). Thus, for Mn- Y substitution with the *later* TMs, $Y = \text{Fe, Co, Ni, Cu}$, the earliest TM is Mn, which therefore remains in $2a$. For this reason, Y will randomly occupy the $4c$ Wyckoff sites. As follows from the present calculations (in the case of $Y = \text{Fe, Co, Ni}$ and also experimentally [19, 20]), such substitution preferably occurs on one of the two $4c$ sites ($2c$ or $2d$; here, let us choose $2d$) by rendering them nonequivalent (see Fig. 1 b). According to the sequence $2a\ 2b\ 2c\ 2d$, we label the resulting compound $\text{MnGaMn}[\text{Mn}_{1-y}\text{Y}_y]$. Statistically, its point symmetry reduces from I_4/mmm to $I-4m2$ (no inversion). Due to similarity with $\text{Mn}(2c/2d)$ the magnetic moments of $Y(2d)$ are coupled negatively to $\text{Mn}(2a)$, i.e., they are oriented up. Since $Y(2d)$ has a smaller magnetic moment compared to $\text{Mn}(2c/2d)$ (because of its more complete d -shell), its partially occupied spin-down subband is downshifted energetically with respect to $\text{Mn}(2c/2d)$, whereas its fully occupied spin-up subband is centered below E_F , similar to the spin-up subband of $\text{Mn}(2c/2d)$. It is clear that such substitution yields the spin-down random fluctuation window including E_F , whereas the spin-up window is situated below E_F (see Fig. 1 b).

A similar effect can be maintained by replacing Mn with earlier TMs: $X = \text{Cr, V, Ti}$ and Sc . According to the aforementioned chemical ordering rules, the earlier TMs occupy the $2a$ Wyckoff site, which is represented in formal notation as $[\text{Mn}_{1-x}\text{X}_x]\text{GaMnMn}$ (see Fig. 1 c). This does not change the I_4/mmm point symmetry. Because of the similarity with $\text{Mn}(2a)$, the magnetic moments of $X(2a)$ are also coupled negatively to $\text{Mn}(4c)$, i.e. are down-oriented. Since the d -shell of the X element is less than half-filled, its spin-up subband is fully

empty (it is situated above E_F), whereas the spin-down subband is partially filled (contains E_F). This again provides two randomly fluctuating energy windows: one including E_F , in the spin-down channel, and the other one, above E_F in the spin-up channel. An additional energy regime of random fluctuations which occurs in the spin-down channel relatively far below E_F exists, which is caused by the deepest fluctuating spin-down subband of $\text{Mn}(2a)$, as shown in Fig. 1 c. Since both substitutions $[\text{Mn}_{1-x}\text{X}_x]\text{GaMnMn}$ and $\text{MnGaMn}[\text{Mn}_{1-y}\text{Y}_y]$ are independent, they can be simultaneously combined into $[\text{Mn}_{1-x}\text{X}_x]\text{GaMn}[\text{Mn}_{1-y}\text{Y}_y]$, as shown in Fig. 1 d. The resulting compound statistically corresponds to the lowest $I-4m2$ symmetry, and its fluctuation spectrum represents a superposition of the energy windows in cases (b) and (c).

III. FIRST-PRINCIPLES JUSTIFICATION

A. Visual analysis of the Bloch spectral function (BSF)

We assume, that the substitution rate, x or y , must be sufficiently small everywhere to prevent noticeable structural or electronic changes. Experimentally, in the case of $Y = \text{Co}$, the critical concentration (when the $\text{Mn}_{3-y}\text{Y}_y\text{Ga}$ composition reaches into the cubic phase) is $y \approx 0.5$; in the case of $Y = \text{Fe}$ or Ni , it is at least $y = 1$ [20]. To date, cases of Mn- X substitution have not been reported apart from $X = \text{V}$, known to be cubic for $x = 1$ [23]. For this reason, among all the cases considered here, the practically interesting examples are those in which the substitution rate does not exceed 10 – 20 % ($0 < x, y \lesssim 0.2$). Nevertheless, since it is interesting to also track the spin-polarization at the disorder rate maximum, we will study $\text{Mn}_{3-y}\text{Y}_y\text{Ga}$ and $\text{Mn}_{3-x}\text{X}_x\text{Ga}$ within a wide range ($0 \leq x, y \leq 0.5$). To examine the effects of the combined substitution (in $\text{Mn}_{3-x-y}\text{X}_x\text{Y}_y\text{Ga}$) we will take $x = y$ but for consistency we will ensure that the sum of these rates does not exceed the maximal rate ($x + y \leq 0.5$). All relevant computational details, including the definition of the Bloch spectral function (BSF) used in the following, are listed in Sec. V.

By comparing the calculated spin-projected BSFs (red and blue indicate spin-up and spin-down, respectively) of Mn_3Ga (Fig. 2 a) with $\text{Mn}_{2.5}\text{Co}_{0.5}\text{Ga}$ (Fig. 2 b) and $\text{Mn}_{2.5}\text{V}_{0.5}\text{Ga}$ (Fig. 2 c), one can identify all the fluctuation regimes (visualized as broadened regions) schematically presented in Fig. 1. In the case of Mn-Co substitution, the random fluctuations in the spin-down channel span a wide energy window $\approx E_F \pm 2$ eV, whereas no broadening is observed for the spin-up states crossing E_F , as the spin-up fluctuations begin only at 1 eV below E_F . In the case of Mn-V, the spin-down fluctuation region is even wider: it roughly spans the -3.5 to 2 eV range as a fluctuating superposition of the lower and higher bands of $\text{Mn}(2a)$ and $\text{V}(2a)$, respectively. Again, almost no broad-

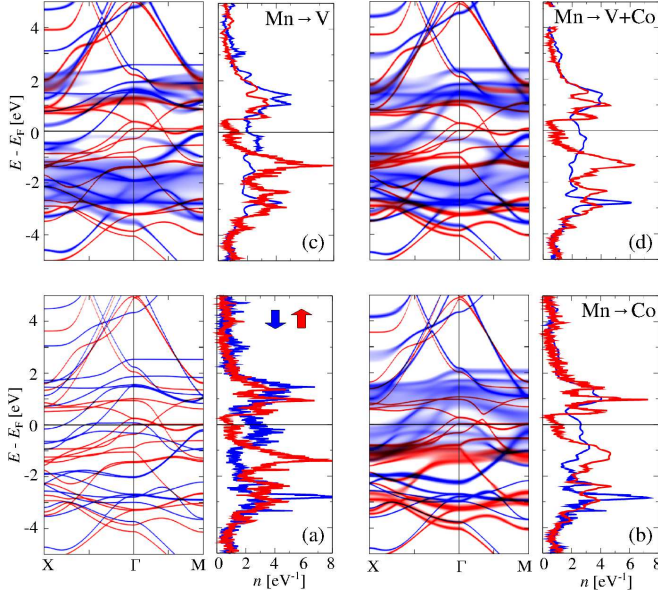


FIG. 2: Spin-projected BSF (red and blue indicate spin-up and spin-down, respectively) along the X- Γ -M path and the spin-projected total DOS computed for (a) MnGaMnMn, (b) MnGaMn[Mn_{0.5}Co_{0.5}], (c) [Mn_{0.5}V_{0.5}]GaMnMn, and (d) [Mn_{0.25}V_{0.25}]GaMn[Mn_{0.25}Co_{0.25}], corresponding to the schemes in Figures 1 a, 1 b, 1 c, and 1 d, respectively.

ening of the spin-up states is observed at E_F , as the spin-up fluctuation window is now shifted above E_F (from 0.5 to 2 eV). In the combined Mn_{2.5}V_{0.25}Co_{0.25}Ga case (Fig. 2d) the fluctuation regime clearly represents a superposition of the fluctuation energy windows in Figs. 2 c and 2 d.

Before we examine to the quantitative estimates, it is instructive to note the difference in informational content provided by the BSF and DOS. In all cases, the spin-resolved DOS indicates that at E_F , $n_F^\uparrow < n_F^\downarrow$, which may lead us to naively assume of a negative spin-polarization, i.e., $P \sim n_F^\uparrow - n_F^\downarrow < 0$. Such an estimate is used quite often, even today. In certain cases, this estimate can be improved upon if, instead of the total DOS, only its s - and p -electron projections are considered, but even such improvement can be efficient only when the electron mobility values in both spin channels are close. In contrast, we see from the BSFs that the electron momentum uncertainties ($\Delta k \sim l^{-1}$) at E_F produced by disorder are also very different for the two spins ($\Delta k^\uparrow < \Delta k^\downarrow$) and suggest the opposite conclusion, i.e., a positive spin-polarization, $P \sim l^\uparrow - l^\downarrow > 0$. Obviously, in such situations, a final conclusion can be made only if it is based on approaches adequately accounting for both factors. For this reason, we compute the spin-projected resistivities as functions of x and y in Mn_{3-x}X_xGa, Mn_{3-y}Y_yGa and Mn_{3-x-y}X_xY_yGa alloys in the following, using the Kubo-Greenwood linear response formalism [24, 25] and applying the relativistic spin-projection scheme [26].

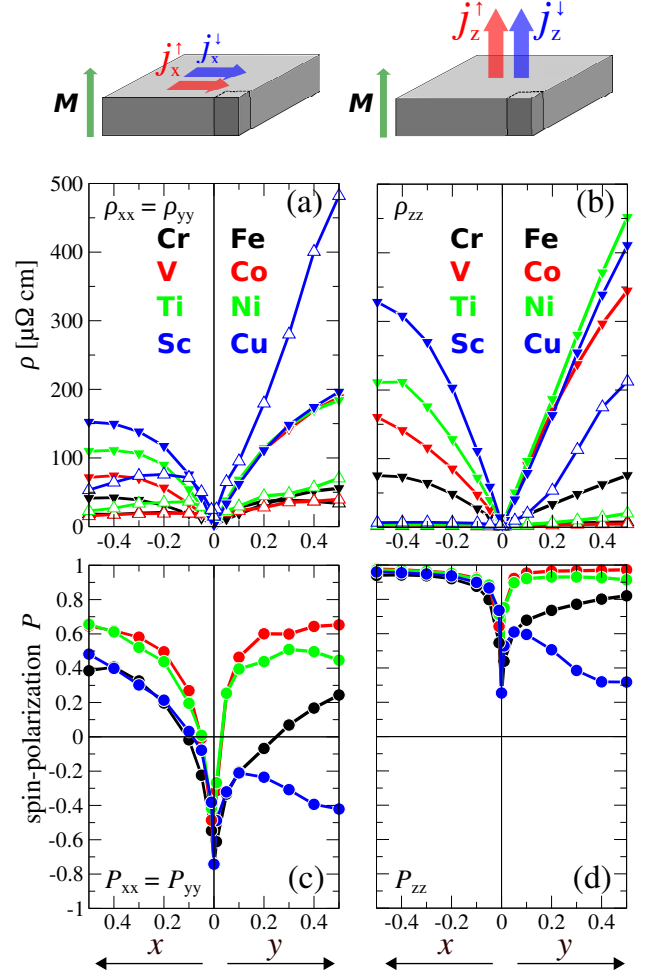


FIG. 3: Spatial components of residual resistivities, $\rho_{xx} = \rho_{yy}$ (a) and ρ_{zz} (b) (their spin-projections, $\rho^{\uparrow(\downarrow)}$, are distinguished by the hollow up- and filled down-oriented triangles), computed as functions of Mn_{1-y}Y_y ($Y = \text{Fe, Co, Ni, Cu}$) and Mn_{1-x}X_x ($X = \text{Cr, V, Ti, Sc}$) random substitutions; the substitution rates x and y increase in the directions indicated by the arrows. Spatial components of spin-polarization, $P_{xx} = P_{yy}$ (c) and P_{zz} (d), are derived from the spin-projections of the corresponding residual resistivity spatial components. The corresponding schemes with electric current, j , magnetization, M , and the unit cell relative orientations are shown above.

B. Quantitative analysis of spin-polarization

Since we examine the tetragonal systems, we will distinguish their properties along the in-plane (xy, or the ab -plane of the tetragonal lattice) and out-of-plane (along z , or the c -axis of the tetragonal lattice) directions. Figures 3a and 3c represent the in-plane transport properties (spin-projected resistivities and spin-polarizations, respectively), whereas Figures 3b and 3d represent the out-of-plane characteristics. In all cases, we assume that M is oriented along the z -axis because of the magnetocrystalline anisotropy. Here, we consider the diagonal

elements of the resistivity tensor, $\rho_{xx} = \rho_{yy} \neq \rho_{zz}$, as being responsible for the direct current, \vec{j} ($j_\alpha = E_\alpha / \rho_{\alpha\alpha}$, \vec{E} is the external electric field and α is the spatial index x, y, or z). The corresponding spatial components of spin-polarization are defined as $P_{\alpha\alpha} = \frac{\rho_{\alpha\alpha}^\downarrow - \rho_{\alpha\alpha}^\uparrow}{\rho_{\alpha\alpha}^\downarrow + \rho_{\alpha\alpha}^\uparrow}$, where $\rho_{\alpha\alpha}^\uparrow, \rho_{\alpha\alpha}^\downarrow$ are the corresponding spin-projections.

As follows from Figs. 3a and 3b, with increasing chemical disorder induced by Mn- X or Mn- Y substitution, almost all spatial/spin resistivity components grow monotonously within $0 \leq x, y \leq 0.5$ (with very few exceptions, e.g., for ρ_{xx}^\uparrow in the case of $X = \text{Sc}$ and Ti at higher x rates, due to a certain increase in n_F^\uparrow). This growth is most efficient for small x or y , and tends to saturate close to $x \approx y \approx 0.5$ (maximal disorder). For the ordered Mn_3Ga , all resistivity components are exactly zero; for this reason, we estimate its spin-polarization by extrapolating corresponding expressions to $x, y \rightarrow 0$. Here, we find that the pure Mn_3Ga represents a rather large spin-polarization spatial anisotropy: $P_{xx} = P_{yy} \approx -0.75$ (Fig. 3c), whereas $P_{zz} \approx +0.25$ (Fig. 3d), which indicates that the spin-polarization estimates for anisotropic systems (e.g., [18]) based on a spin-resolved DOS at E_F can be improved by considering the spatially-resolved DOS in momentum space. The resistivity spin component trends as functions of x and y show that ρ^\downarrow grows faster than ρ^\uparrow , which essentially justifies the proposed scheme (see Sec. II). Indeed, both P_{xx} and P_{zz} , as functions of x or y , evolve towards larger positive values. The absolute disorder-induced change of the P_{xx} component is very large, from -0.75 to approximately $+0.65$ (for Mn-Ti, Mn-V, and Mn-Co substitutions), i.e. $\Delta P_{xx} \approx 1.4$. Despite the fact that this particular effect is not especially interesting, since absolute spin-polarization does not increase, it clearly demonstrates the importance of disorder.

An interesting point worth mentioning is that the disorder influence is stronger for those alloys in which the substituting type (X or Y) is further from Mn (e.g., in terms of the group or valence electrons number), i.e., a larger potential difference leads to a stronger random fluctuation amplitude. Indeed, for the types “closest” to Mn, i.e., $X = \text{Cr}$ and $Y = \text{Fe}$, the corresponding resistivity components are comparably small (e.g., at $x = y = 0.5$): $\rho_{xx}^\uparrow : 18 \sim 33$, $\rho_{xx}^\downarrow : 41 \sim 55$, $\rho_{zz}^\uparrow : 2.3 \sim 7.5$, and $\rho_{zz}^\downarrow : 75.3 \sim 75.7 \mu\Omega\text{cm}$. At the same time, for the types “most distinct” from Mn, i.e., $X = \text{Sc}$ and $Y = \text{Cu}$, certain resistivity components are much larger, but not always comparable: $\rho_{xx}^\uparrow : 53 \sim 481$, $\rho_{xx}^\downarrow : 152 \sim 197$, $\rho_{zz}^\uparrow : 6.9 \sim 212$, and $\rho_{zz}^\downarrow : 327 \sim 411 \mu\Omega\text{cm}$. This simply indicates that, whereas substitution of Mn with “too similar” elements is not yet appropriately efficient, substitution with “too distinct” elements rapidly escapes control, since the band structure is strongly affected not only in the sense of the Bloch-wave broadening, but also in the sense of dispersion, E_F position, etc. The most inefficient situation is observed for Mn-Cu substitution. Here, ρ^\uparrow and ρ^\downarrow grow rapidly by achieving large absolute values,

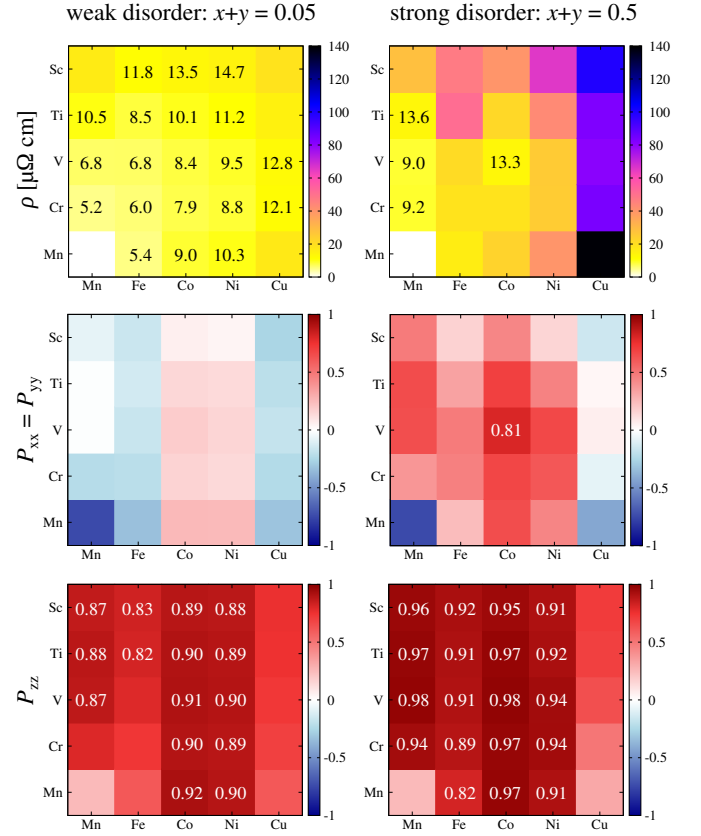


FIG. 4: Residual resistivities, ρ , (averaged over spins and spatial directions) and spin-polarization spatial components ($P_{xx} = P_{yy}$, within xy-plane; P_{zz} , out-of-plane) calculated for $\text{Mn}_{3-x-y}\text{X}_x\text{Y}_y$ compositions ($X = \text{Cr}, \text{V}, \text{Ti}, \text{Sc}$; $Y = \text{Fe}, \text{Co}, \text{Ni}, \text{Cu}$; formally, we also include Mn). The total amount of substituted Mn is fixed to either $x + y = 0.05$ (weak disorder, left-side) or to $x + y = 0.5$ (strong disorder, right-side). Thus, for the strong disorder, if, for example, $x = 0$, then $y = 0.5$, and vice versa, or if both $x, y > 0$, then $x = y = 0.25$. For the compositions with $P > 0.8$ and $\rho < 15 \mu\Omega\text{cm}$, the corresponding values are shown explicitly.

but their ratios, and, thus, the spin-polarization, remain unsatisfactorily low. In contrast, substitution with “intermediate” elements, $X = \text{V}, \text{Ti}$, or $Y = \text{Co}, \text{Ni}$, appears to be very efficient. Specifically, at $x, y \approx 0.1$ the out-of-plane spin-polarization achieves $P_{zz} \approx 0.91 - 0.95$ and grows further with increased disorder rate. As follows from Fig. 3b, such growth is mainly due to the increase of the ρ_{zz}^\downarrow component, whereas ρ_{zz}^\uparrow remains almost unaffected, as was supposed in Sec. II during the discussion of the constructive disorder design.

In order to also study the combined effects (in $\text{Mn}_{3-x-y}\text{X}_x\text{Y}_y$ compositions), we plot the computed transport characteristics, $P_{xx} = P_{yy}$ and P_{zz} , together with the spatially- and spin-averaged (effective) resistivity, $\rho = (2\rho_{xx} + \rho_{zz})/3$, where $\rho_{\alpha\alpha} = 1 / (1/\rho_{\alpha\alpha}^\uparrow + 1/\rho_{\alpha\alpha}^\downarrow)$ is computed for the weak ($x + y = 0.05$) and strong ($x + y = 0.5$) disorder regimes, as shown in Fig. 4. It can be seen that, by moving towards Sc and Cu, the

effective resistivity tends to increase. In both disorder regimes this larger resistivity is exhibited by all Cu-containing compositions, with a maximum of approximately $140 \mu\Omega\text{cm}$ for the $\text{Mn}_{2.5}\text{Cu}_{0.5}\text{Ga}$ alloy. At the same time, the spin-polarization of metals with large resistivity is always low, since the spin component with higher resistivity cannot go far beyond the Mooij limit, whereas the other spin component with lower resistivity is already sufficiently high enough. On the other hand, alloys with lower effective resistivities, such as Co- or V-containing compositions, exhibit much higher spin-polarization. Interestingly, they show a noticeable “complementary” effect, seen for example in the strongly disordered regime; whereas for both $\text{Mn}_{2.5}\text{Co}_{0.5}\text{Ga}$ and $\text{Mn}_{2.5}\text{V}_{0.5}\text{Ga}$, $P_{xx} \approx 0.65$, for the combined composition, $\text{Mn}_{2.5}\text{V}_{0.25}\text{Co}_{0.25}\text{Ga}$, it is already 0.81. It is also instructive to admit the efficiency of the constructive disorder; by moving from Mn_3Ga through the weakly disordered $\text{Mn}_{2.95}\text{V}_{0.025}\text{Co}_{0.025}\text{Ga}$ to $\text{Mn}_{2.5}\text{V}_{0.25}\text{Co}_{0.25}\text{Ga}$, which is the ten times more strongly disordered, P_{zz} evolves from 0.25 through 0.91 to 0.98, respectively. This means that, in order to achieve high spin-polarization, the small substitution rate is already sufficient.

IV. SUMMARY AND OUTLOOK

As we have seen, an increase in spin-polarization is observed almost for any type of Mn-TM substitution within Mn_3Ga , beginning with Sc and ending with Ni. The exception is the Mn-Cu case, which leads to a very strong random potential fluctuation affecting both spin channels. The important feature of Mn_3Ga is its tetragonal structure, which causes a large anisotropy in its transport characteristics. As a result, the spin-polarization along the in-plane and out-of-plane directions evolves differently. Whereas the disorder-induced change is strong in both directions, it is the most constructive in the out-of-plane direction only. At the same time, the constructive effect is achieved immediately, by beginning with a small Mn-TM substitution rate. This is suitable for spintronics elements exploiting magneto-resistance effects, as the unnecessarily high resistance of the electrodes produces unwanted energy losses. Another positive aspect of the presented scheme is the improvement in spin-polarization specifically for the “current-perpendicular-to-plane” (CPP) setup. This improvement in combination with perpendicular magnetic anisotropy is applicable to many state-of-the-art industrial developments. On the other hand, this also means that the direct experimental proof of the proposed scheme, at least on a Mn_3Ga

basis, requires preparation of the single-crystalline structures with effective stoichiometric control, which is rather sophisticated. In this respect, an interesting future focus is constructive disorder design in cubic systems, as high spin-polarization can be expected in the isotropic case even for polycrystalline materials. As we have seen, the basic feature which provides the necessary conditions for such disorder engineering, is the presence of two antiparallel magnetic sublattices. Hence, suitable cubic candidates for this research can be found within the same Mn-rich Heusler group.

V. APPENDIX

All the present computations were performed using the fully relativistic SPR-KKR (spin-polarized relativistic Korringa-Kohn-Rostoker) Green’s function method, using the generalized gradient approximation (GGA) in a form proposed by Perdew, Burke and Ernzerhof (PBE) [27]. The chemical disorder was treated within the CPA [13, 14], as implemented in SPR-KKR. The electronic structure is represented via the Bloch spectral function (BSF), defined as a Fourier transform of the real-space Green’s function $G(\vec{r}, \vec{r}', E)$ with

$$A(\vec{k}, E) = -\frac{1}{\pi N} \text{Im} \sum_{n,m=1}^N e^{i\vec{k}(\vec{R}_n - \vec{R}_m)} \times \int d^3r \left\langle G(\vec{r} + \vec{R}_n, \vec{r} + \vec{R}_m, E) \right\rangle,$$

where $\langle \rangle$ is the CPA average and $\vec{R}_{n,m}$ are the atomic site coordinates. $A(\vec{k}, E)$ can be interpreted as a \vec{k} -resolved DOS function, since

$$n(E) = \frac{1}{\Omega_{\text{BZ}}} \int_{\Omega_{\text{BZ}}} d^3k A(\vec{k}, E),$$

with $n(E)$ indicating the total DOS function, and Ω_{BZ} the Brillouin zone volume.

Acknowledgments

Financial support from the Deutsche Forschungsgemeinschaft (DfG) (research unit FOR No. 1464 “ASPI-MATT”, project P 1.2-A) and European Research Council Advanced Grant (ERC-AG) No. 291472 “IDEA Heusler” is gratefully acknowledged.

-
- [1] W. F. Smith and J. Hashemi, *Foundations of Materials Science and Engineering (3d edition)* (McGraw-Hill, 2004).
 [2] J. Pierre, B. Dollet, and V. Leroy, Phys. Rev. Lett. **112**,

148307 (2014).

- [3] L. Sapienza, H. Thyrestrup, S. Stobbe, P. D. Garcia, S. Smolka, and P. Lodahl, Science **327**, 1352 (2010).
 [4] P. W. Anderson, Phys. Rev. **109**, 1492 (1958).

- [5] D. J. Thouless, Phys. Rep. C **13**, 93 (1974).
- [6] J. Li, R.-L. Chu, J. K. Jain, and S.-Q. Shen, Phys. Rev. Lett. **102**, 136806 (2009).
- [7] C. W. Groth, M. Wimmer, A. R. Akhmerov, J. Tworzydło, and C. W. J. Beenakker, Phys. Rev. Lett. **103**, 196805 (2009).
- [8] H. Jiang, L. Wang, Q.-F. Sun, and X. C. Xie, Phys. Rev. B **80**, 165316 (2009).
- [9] N. Mott, Proc. Roy. Soc. (London) A **153**, 699 (1936).
- [10] J. H. Mooij, Phys. Stat. Sol. (a) **17**, 521 (1973).
- [11] J. Kübler, A. R. Williams, and C. B. Sommers, Phys. Rev. B **28**, 1745 (1983).
- [12] R. A. de Groot, F. M. Mueller, P. G. van Engen, and K. H. J. Buschow, Phys. Rev. Lett. **50**, 2024 (1983).
- [13] P. Soven, Phys. Rev. **156**, 809 (1967).
- [14] W. H. Butler, Phys. Rev. B **31**, 3260 (1985).
- [15] W. Metzner and D. Vollhardt, Phys. Rev. Lett. **62**, 324 (1989).
- [16] G. Kotliar, S. Y. Savrasov, K. Haule, V. S. Oudovenko, O. Parcollett, and C. A. Marianetti, Rev. Mod. Phys. **78**, 865 (2006).
- [17] P. J. Webster, Contemp. Phys. **10**, 559 (1969).
- [18] J. Winterlik, B. Balke, G. H. Fecher, C. Felser, M. C. M. Alves, F. Bernardi, and J. Morais, Phys. Rev. B **77**, 054406 (2008).
- [19] V. Alijani, J. Winterlik, G. H. Fecher, and C. Felser, Appl. Phys. Lett. **99**, 222510 (2011).
- [20] J. Winterlik, S. Chadov, A. Gupta, V. Alijani, T. Gasi, K. Filsinger, B. Balke, G. H. Fecher, C. A. Jenkins, F. Casper, et al., Adv. Materials **24**, 6283 (2012).
- [21] K. Rode, N. Baadji, D. Betto, Y.-C. Lau, H. Kurt, M. Venkatesan, P. Stamenov, S. Sanvito, J. M. D. Coey, E. Fonda, et al., Phys. Rev. B **87**, 184429 (2013).
- [22] P. W. Anderson, Phys. Rev. **124**, 41 (1961).
- [23] K. R. Kumar, N. H. Kumar, G. Markandeyulu, J. A. Chelvane, V. Neu, and P. Babu, J. Magn. Magn. Materials **320**, 2737 (2008).
- [24] R. Kubo, J. Phys. Soc. Japan **12**, 570 (1957).
- [25] D. A. Greenwood, Proc. Phys. Soc. **71**, 585 (1958).
- [26] S. Lowitzer, D. Ködderitzsch, and H. Ebert, Phys. Rev. B **82**, 140402(R) (2010).
- [27] J. P. Perdew, K. Burke, and M. Ernzerhof, Phys. Rev. Lett. **77**, 3865 (1996).